Available online at www.sciencedirect.com

SciVerse ScienceDirect

Advances in Space Research 52 (2013) 403–411

ADVANCES IN SPACE RESEARCH (a COSPAR publication)

www.elsevier.com/locate/asr

Fading in the HF ionospheric channel and the role of irregularities

C. Bianchi *, J.A. Baskaradas, M. Pezzopane, M. Pietrella, U. Sciacca, E. Zuccheretti

Istituto Nazionale di Geofisica e Vulcanologia, Via di Vigna Murata 605, 00143 Rome, Italy

Available online 11 April 2013

Abstract

It is well known that the ionosphere affects radio wave propagation especially in the high frequency (HF) range. HF radio waves reflected by the ionosphere can reach considerable distances, often with changes in amplitude, phase, and frequency. The ionosphere is a dispersive in frequency and time, bi-refractive, absorbing medium, in which multipath propagation due to traveling irregularities is very frequent. The traveling irregularities undulate the reflecting ionospheric layer, introducing variations in signal amplitude (fading). In this multipath time variant channel fading is mainly considered, even though it is not the sole effect. Echo signals from a single reflection, as in ionospheric vertical sounding (VIS) techniques, are affected by a certain degree of variability even in quiet ionospheric conditions. In this work the behavior of the ionospheric channel is studied and characterized by observing the power variation of received echoes using the VIS technique. Multipath fading was analyzed quantifying the power variation of the signal echo due to irregularities on a temporal scale from 0.5 to 256 s. An experimental set-up derived from an ionosonde was implemented and the analysis was performed employing a special numerical algorithm operating off-line on the acquired time sequence of the signal. The gain-loss of the irregularity shapes are determined in some special cases.

Keywords: Fading fluctuation; Ionospheric irregularities; Multipath time-variant channel

1. Introduction

High frequency (HF) radio-wave propagation relies on the presence of ionospheric reflecting layers to overcome the Earth's curvature. In long-range communications, several technological applications of remote sensing and sky-wave radar operating in the HF frequency range often require particularly quiet ionospheric conditions for relatively long time periods. This requirement contrasts with the time and coherence bandwidth of the ionospheric channel which is degraded by multipath propagation and the time varying channel (Sklar, 2001). Hence, to understand the behavior of the channel, and how it affects HF signals in modern technological wide broadband applications (spread spectrum and multicarrier radio, sky wave radar, etc.) (Proakis, 1995), it has become important to evaluate these effects. For the same reason, to maintain an adequate performance in wide bandwidth HF radar systems and other remote sensing applications requires reliance on stable ionospheric reflection for relatively long time periods, while in contrast a time varying multipath channel produces fading in the signal as one of the most obvious effects.

Since the first HF radio wave applications, ionospheric physicists have known that even in quiet conditions the echo signal is subject to variability due to irregularities that in the extent of infrasonic disturbances are unpredictable, because of the large variety of triggering sources (Blanc 1985). Large scale and medium scale traveling ionospheric disturbances (LS and MS TIDs) heavily perturb the ionosphere. These phenomena have been described (Hines, 1960; Francis, 1975; Krasnov et al., 2006) and they are the ionospheric manifestation of acoustic gravity waves (AGW) (Crowley and Rodrigues, 2012). This paper addresses small scale disturbances (SSD) with a 0.5–250 s time period, which quite often do not travel in an organized and coherent way. These irregularities have been studied mainly considering variations in electron density and virtual heights of iso-density surfaces of the investigated

* Corresponding author. Tel.: +39 0651860326; fax: +39 0651860397.
E-mail address: cesidio.bianchi@ingv.it (C. Bianchi).

0273-1177/$36.00 © 2013 COSPAR. Published by Elsevier Ltd. All rights reserved.
http://dx.doi.org/10.1016/j.asr.2013.03.035

ionospheric region. This is because the available data derive from traditional ionospheric vertical sounding, drawn from the huge worldwide database (Reinisch and Galkin, 2011). Ionogram parameters, mainly electron density and virtual height, as well as foF2, M(3000)F2, and MUF(3000)F2, have been widely studied and the periodicity compared with the SSD on a space-time scale (among others, Kouris et al., 2000). There are other simple techniques and methods much more effective for highlighting different reflector characteristics, such as the shape of the reflector and its evolution in time. In this controlled experiment, by means of range gating selection, the reflecting area illuminated by the antenna's beam is reduced, thus filtering out the signal from distant reflectors. It is worth noting that geometric variation losses are only a fraction of a dB by applying a range gating of the order of tens of km. For the same reason ionospheric absorption can also be ignored because it can be assumed to be approximately constant during the acquisition time. The main factors in the fading of HF signals propagating in the ionosphere are: polarization, amplitude effects due to focusing and defocusing, and multipath.

Fading due to polarization occurs because of the rotation of the electric vector (Faraday rotation). Moreover, due to the bi-refractive property of the ionosphere, a linearly polarized wave will split into two characteristic waves, the ordinary and the extraordinary, circularly polarized in opposite directions, which propagate in the ionosphere with different paths and speeds. Consequently the resultant linear polarization at the receiver is different relative to the initial polarization. Polarization fading (James et al., 2006) is not considered in this work because the low frequency waves employed in the experimental arrangement do not deeply penetrate the ionospheric region investigated and do not split into ordinary and extraordinary waves. For the same reason Faraday rotation is ignored even though in general this type of fading can produce losses from 0 to a few dB (McNamara, 1991). Finally, it is also useful to ignore Doppler frequency shifts since the vertical velocity of the SSD and MSTID is small compared to the horizontal velocity. In any case, the latter does not make significant contributions because the component along line of sight (LOS, nearly vertical) is small. That leaves only multipath fading produced by irregularities and fading due to the focusing–defocusing effects of the reflector shape. Considering the irregular time changing contours of the iso-density surfaces, statistically it is rare to have only one flat reflector. Instead, reflectors showing a convex or concave shape, producing respectively further gain or loss to the signal (Bianchi et al., 2003), are expected.

2. Vertical sounding measurements and characterization of analytical signal

In order to characterize echo signal fading in the specific case of vertical propagation, an experimental set-up able to measure power and virtual height (PVH) of ionospheric reflectors was prepared. The measurement was performed using the AIS-INGV ionosonde (Zuccheretti et al., 2003) which is a low power HF radar based on the pulse compression technique with a mathematical processing gain of 25 dB. About 13 dB derive from the correlation process while the remainders are related to coherent integration (Bianchi et al., 2013). To achieve this a complementary phase code of 16 chips modulates the sine wave carrier. The modulated carrier with a peak power of hundreds of watts is sent into the ionosphere by means of a low gain, long wire cross coupled delta antennas. The system records power (dBm) and virtual height (km) value pairs for the highest signal peak returning from the ionosphere. However, the power of the signal at the receiver input required system calibration for this experimental set-up. Routine ionosonde measurements were scheduled every 15 min and lasted approximately 180 s. A PVH measurement session was started after normal sounding and lasted 256 s, consequently the PVH measurement session was also repeated every 15 min. Also in basic vertical sounding measurements the height of the ionospheric layers is one of most important parameters and in the following analysis it is always compared with the PVH. Hence, from the received echo it is possible to derive a peak, the position and amplitude of which are related to the virtual height of reflection and the received power, respectively (see Fig. 2 of Bianchi et al., 2013).

In order to achieve a favorable signal-to-noise ratio (S/N) from the ionosphere, after correlation an integration process is necessary. Because of the time varying nature of the ionosphere or ionospheric coherence time, a very short time period was adopted for integration. A Coherent integration time (CIT) equal to 0.5 s is reasonably less than the supposed time stability of the ionosphere (from 0.5 s to some tens of seconds). This means that each PVH pair is provided every 0.5 s after 30 integrations working at 60 pulses per second. PVH measurements were performed at the Rome ionospheric observatory (Italy, 41.8° N, 12.5° E), collecting a series of data during the period from 3 to 22 January 2008 in the time interval between two vertical ionospheric soundings (VIS), to exactly define the ionospheric layer investigated. Over the whole measurement campaign 1920 time sequences of PVH data were acquired. Before active sounding the noise level at the process output was also analyzed at the various times of the day during the campaign period. The environmental and internal electrical radio noise was recorded above the 66 kHz band, this being the bandwidth of the receiver. Over the whole campaign the noise level after the process, i.e. after 30 integrations of duration 0.5 s, was always less than −94 dBm. Furthermore, the sharp peaks allow the required accuracy to be obtained without ambiguity (±0.5 dB for the power and ±5 km for the virtual height). For this purpose a computer program (Pietrella and Zuccheretti, 2010) was employed to select and analyze the data, determining the time periodicity of fading fluctuation and the intensity of the phenomena.

To analyze the received echo signal, the following relation was considered:

$$r(t) = \sum_{i=0}^{M} \alpha_i(t) \cdot u(t - \tau_i(t)) \cdot \cos\{2\pi f_0[t - \tau_i(t)] + \varphi_i(t)\} + N(t), \quad (1)$$

where t is the time, $\tau_i(t)$ the time dependent delay, f_0 is the carrier frequency, $\alpha_i(t)$ is the attenuating factor of the ith path, that assumes values from 0 to 1, $\varphi_i(t)$ is the phase, $u(t-\tau_i(t))$ is the waveform, dependent on the time delay $\tau_i(t)$, $N(t)$ is the noise and M the number of paths dependent on time; $r(t)$ is then a sum of time delayed attenuated frequency shifted replica of the emitted signal having envelope $u(t)$ that contains the bi-phase code (Bianchi and Altadill, 2005). Of course, the composite signal can experience a Doppler frequency shift that changes the phase according to $2\pi f_0[\mathrm{d}\tau_i(t)/\mathrm{d}t]\ t$, due to the moving reflectors, causing as a consequence short time scale variations of the power of the received echo. This is neglected in the present paper together with the term $\varphi_i(t)$ for the reasons explained above. The effects of noise are also ignored, because they are much less relevant than the multipath contribution. With these assumptions, the echo signal is then down converted to the baseband by an in-phase and quadrature detection as described by the following relation:

$$y(t) = \sum_{i=0}^{M} \alpha_i(t) \cdot u(t - \tau_i(t)); \quad (2)$$

$y(t)$ can be recognized as the output of a system characterized by an impulsive channel response $h(\tau, t) = \sum_{i=0}^{M} \alpha_i(t) \cdot \delta(t - \tau_i(t))$. The sampling of signal (2), using a sampling frequency $f_s = f_0$, produces a time discrete sequence $y_n = y(t_n)$ that can be expressed mathematically as in the following:

$$y_n = \sum_{i=0}^{M} \alpha_i(t_n) \cdot u(t_n - \tau_i(t_n)); \quad (3)$$

this is the attenuated composite envelope signal whose components have different times of arrival (multipath components), whose different phases interfered in constructive or destructive ways. After acquisition, the correlation process (in the frequency domain) and coherent integration are conducted. These two processes can be expressed by the following equations, naming COR_m (the output of the correlator), and I_k (the output of the coherent integrator):

$$COR_m = Y_m \cdot U_m^*, \quad (4)$$

$$I_k = \sum_k COR_{k,m}, \quad (5)$$

where Y_m and U_m^* (where m represents the $m-$ith spectral component) are the Fast Fourier Transform (FFT) of the received signal and the code FFT complex conjugate, while k is the integration sum index. Finally, inverse FFT is performed on the integrated signal to return to the time domain. What emerges from the noise and the unavoidable side lobes is a series of narrow peaks (pulse compression) due to the echoes from the ionospheric reflectors, with an overall processing gain of about 25 dB.

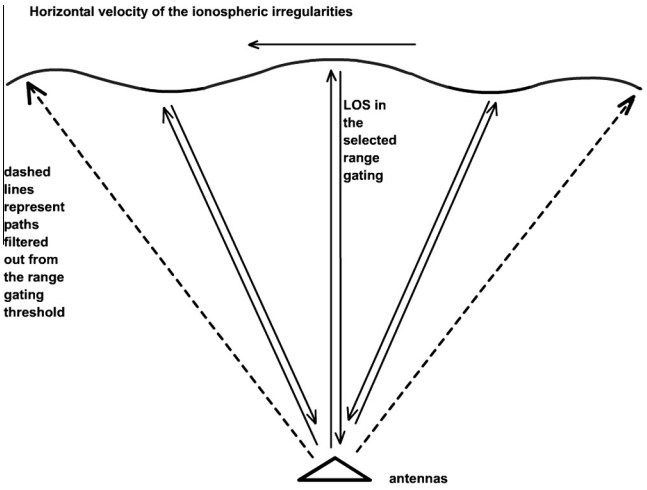

Fig. 1. The horizontal velocity components projected along the line of sight are not significant only for dashed line paths filtered out by the range gating threshold.

3. Traveling ionospheric irregularities

Multipath fading is caused by the presence of different propagation time varying paths between the transmitter and receiver. The waves from these different paths can interfere constructively or destructively depending on the phase difference at the receiving point. Due to the dynamic nature of the ionosphere, the phase difference between the

Table 1
TID classes according to their horizontal scales (from Crowley and Rodrigues (2012)).

Scale-irregularities	Spatial scale (km)	Period (minutes)	Horizontal phase velocity (m/s)	Associated fading
SSD: small-scale disturbances (infrasonic variability)	<100	<10	<50	Multipath fading Less relevant focusing–defocusing phenomena
MSTID: medium scale traveling ionospheric disturbances	100–300	10–30	50–300	Amplitude fading Focusing–defocusing
LSTID: large scale traveling ionospheric disturbances AGW	300–3000	30–300	300–1000	Amplitude fading Focusing–defocusing Deep fading due to ionospheric tilt

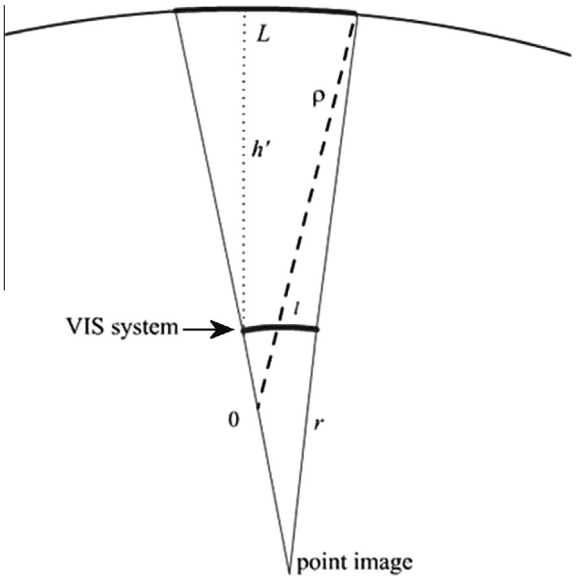

Fig. 2. Geometry of reflection in the VIS technique. L is the section of the area illuminated by the antenna, l is the section of the area at the level of ground where the power is concentrated, h' is the virtual height of reflection (approximately constant), r is the distance of the point-image from the arc, and ρ is the radius of curvature of the spherical reflector (from Whitehead, 1956).

different waves will vary over time, and therefore cause signal fading at the receiver. When the ionosphere is perturbed, the numerous reflecting points can produce time varying fading of periodicities from a few seconds to tens of seconds according to the scale of the irregularities. There is another contribution that induces fading, mainly due to focusing effects due to the movement of LS irregularities that produce slower fading starting from tens of seconds. In fact, the motion of LS irregularities in the ionosphere causes amplitude fading unlike phase interference fading. Depending on the position and the shape of the irregularities, the ionosphere acts like a mirror for HF waves. When radio waves are reflected from a concave iso-density surface, the waves will undergo a focusing gain; conversely, when the surface is convex, there is a loss due to the defocusing effect. Table 1 shows the scale of irregularities with associated phenomena (Crowley and Rodrigues, 2012; Leitinger and Rieger, 2005).

Fig. 1 schematically shows the experimental measurements configuration. It is possible to infer the negligible effect of the Doppler influence on the signal in this peculiar condition of nearly vertical LOS (Crowley and Rodrigues, 2012). As will be seen in the next section, it is possible to ignore the term of the frequency shift in the analytic description. For instance, when the height is 100 km, applying a threshold of 10 km enables investigation of an ionospheric surface of hundreds of square km. In general, different propagation modes or paths in the ionosphere have different amplitudes, polarization, group delays, etc. When describing the ionospheric propagating channel these phenomena must be considered even at mid-latitudes (Warrington et al., 2009). They produce signal deterioration especially in new techniques employed in HF communication (Sklar, 2001) that stress the time variant wide band ionospheric channel. Even in narrow band channels

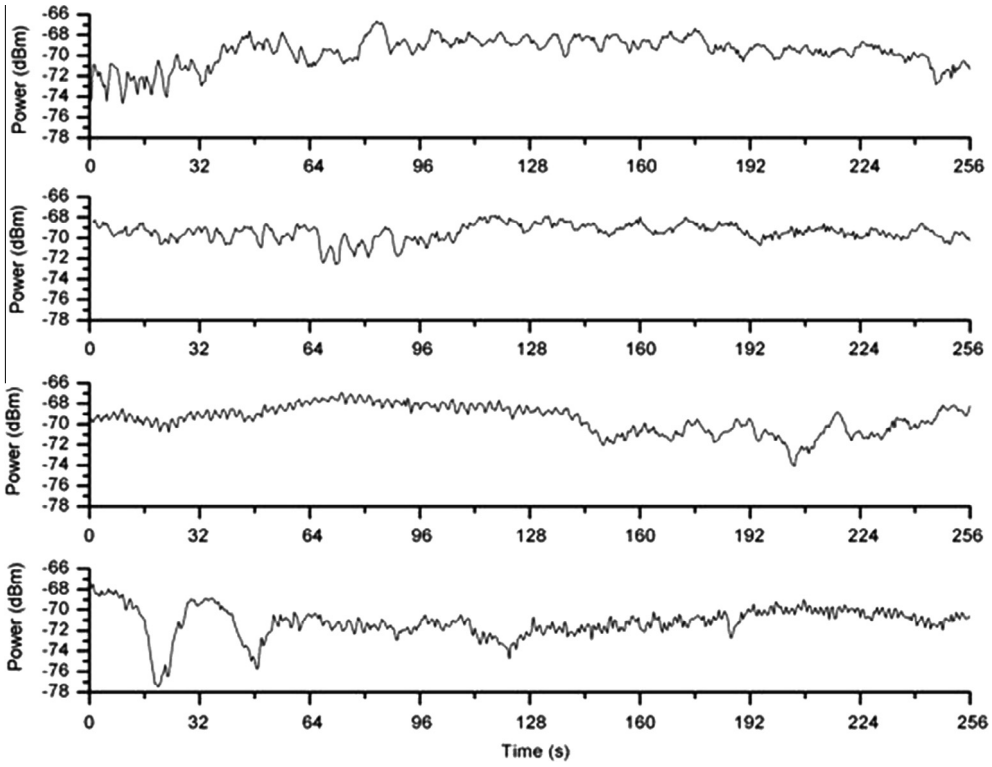

Fig. 3. Signals reflected from the F-layer during the time period between 13:00 and 14:00 UT.

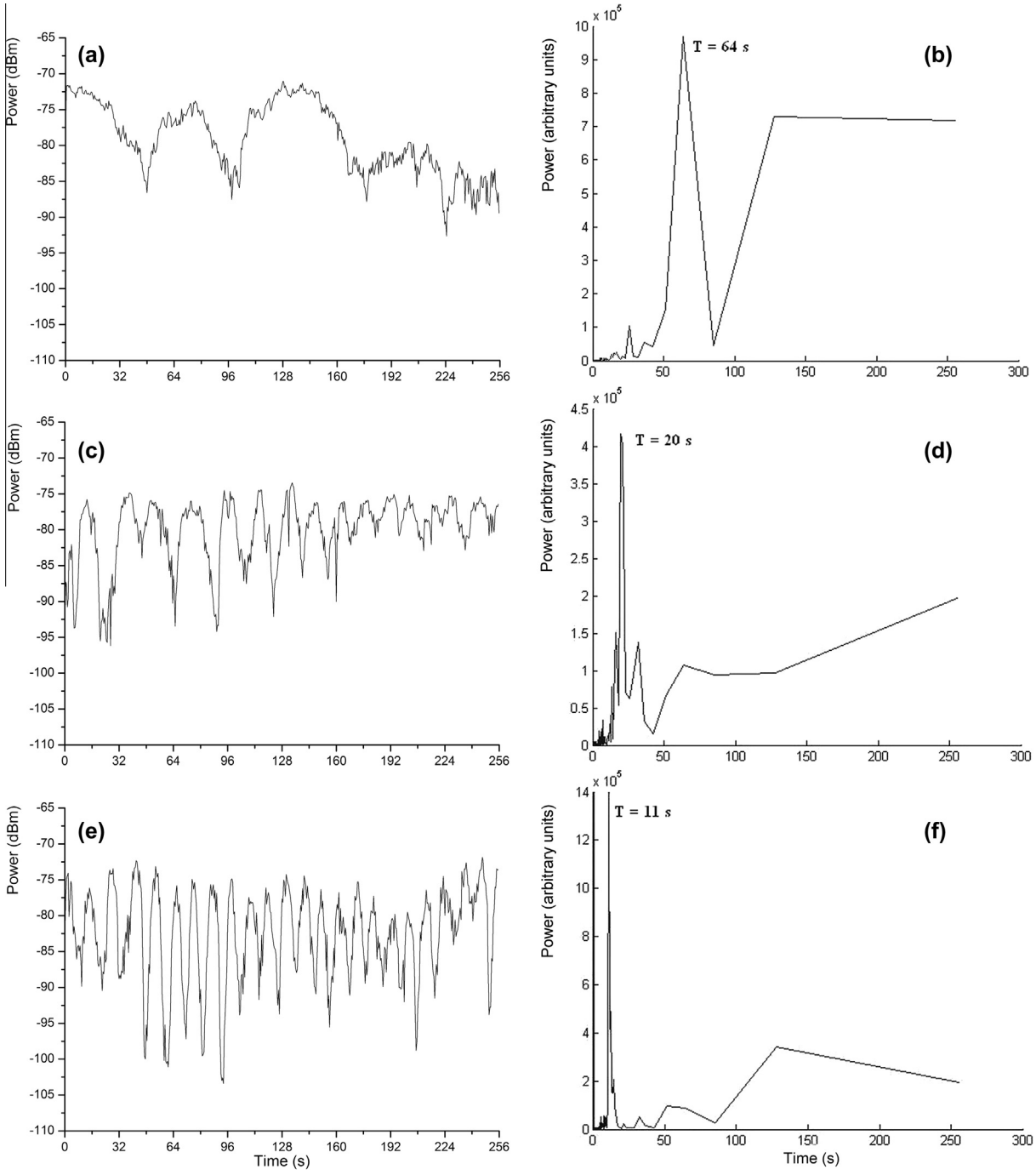

Fig. 4. (a), (c) and (e) Rayleigh fading observed over a time interval of 256 s and (b), (d) and (f) the corresponding periodograms obtained by the FFT analysis.

the amplitude and phase of the propagating wave are time dependent and produce fading at various time scales. High or low latitude propagation paths further influence the intensity of the effects as well as the presence of sporadic-E (Es) layer (Blaunstein and Plohotniuc, 2006).

If HF communication systems do not exploit a wide band, they are less affected by these problems, while degradation in OTHR (over the horizon radar) systems could be more relevant because of the Coherent Integration Time (CIT) and coherence bandwidth degradation (Yau et al., 2006). The ionospheric time-varying channel produces phase, amplitude, and frequency spreading and distortions of the received signal, degrading the performance of OTHR and HF radar for geophysical applications, especially when CITs last several seconds. During this time the phase of the received signal must not exceed 90°, otherwise the CIT becomes ineffective. Statistically, the ionospheric channel exhibits a Nakagami–Rice or Rayleigh

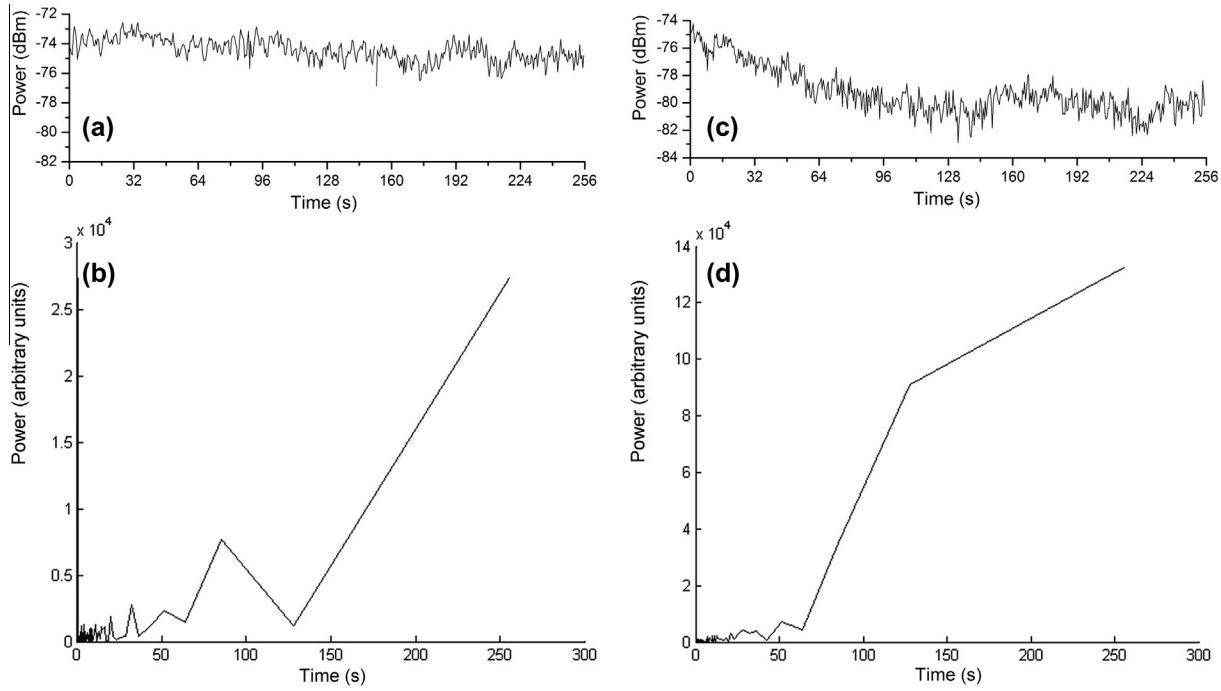

Fig. 5. (a) and (c) Nagakami–Rice fading observed over a time interval of 256 s and (b), (d) the corresponding periodograms obtained by the FFT analysis presenting no well-defined periodicities.

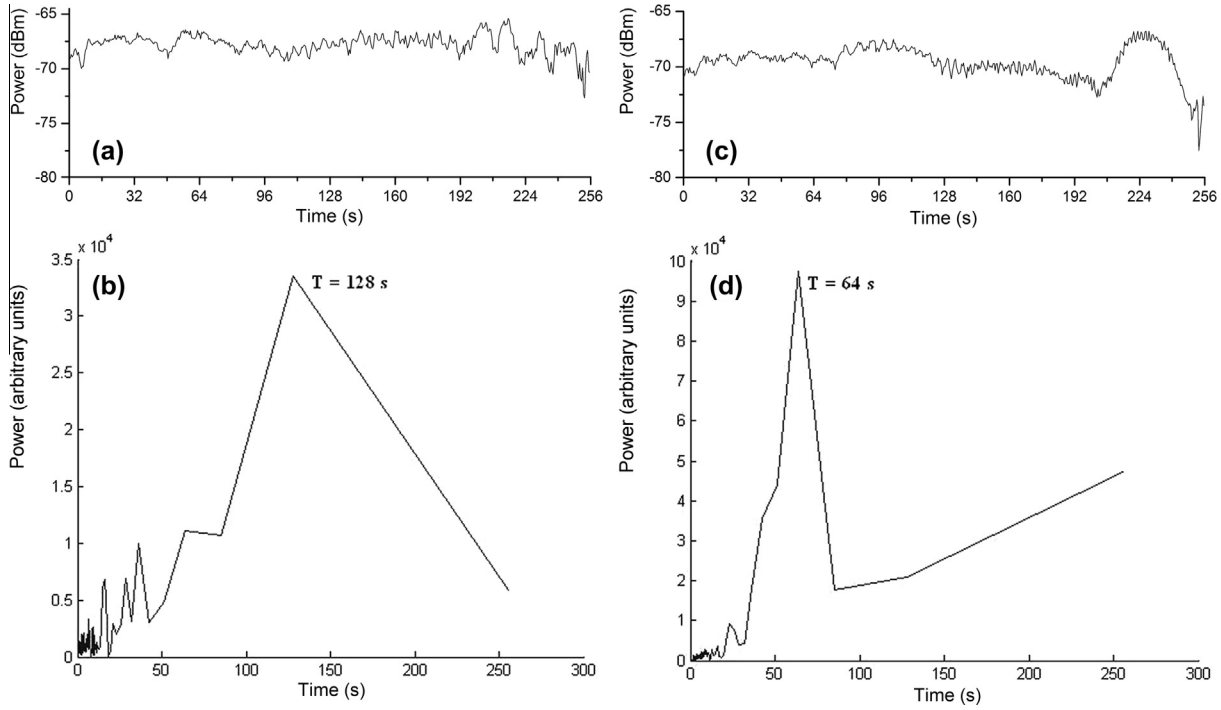

Fig. 6. (a) and (c) Examples of mixed statistical fading trends observed over a time interval of 256 s and (b) and (d) the correspondent periodograms obtained by the FFT analysis

fading trend, depending on the time and spatial scale of the disturbances that are present in the medium during propagation (Sklar, 2001). As shown in Fig. 1, irregularities in TIDs produce iso-density surface motions and undulation with multipath phenomena in the received signal. So, at a receiving point, the composite signal contains a sum of multipath components as described in (3), reflected back from the illuminated ionospheric reflectors.

According to the scheme in Fig. 1, the transmitter illuminates hundreds of square km because of the low gain antenna (3 dB center of the band). With a range gating selection after the acquisition of the signal, it is possible

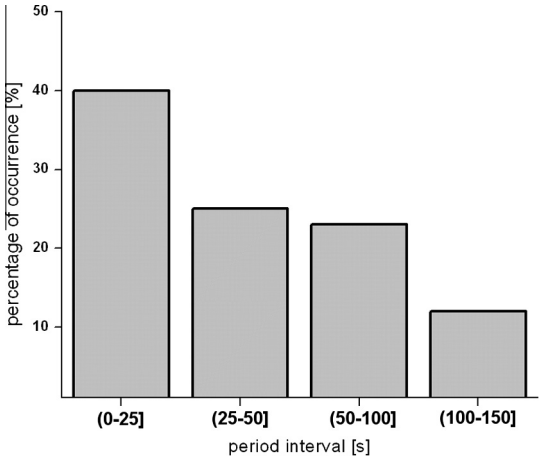

Fig. 7. Percentage of occurrence of the main periods found analyzing the periodograms given as output by the FFT analysis performed on PVH sequences of echo signals for a generic (Rayleigh, Nagakami–Rice or mixed) ionospheric channel.

to reject unwanted echoes from iso-density ionospheric surfaces that can interfere with the ionospheric region under investigation. The bottom of the ionospheric reflector is of great interest in this study because the low frequency employed does not penetrate greatly into the plasma, remaining within the constraint explained at the end of section 1.

4. Shaped coherent reflectors produced by irregularities

Traveling irregularities deform the flat ionospheric layering in various ways producing shaped rippled surfaces. These reflecting iso-density surfaces often comprise different areas with concave and convex faces which can act as focusing or defocusing mirrors, and the received signal power varies according to the extent and curvature of the surfaces. For a convex cylindrical or spherical cap, adopting 2-D and 3-D models and exploiting a simple law of optical geometry, the reflector gain can be determined. Referring to Fig. 2, the radar system is positioned at a distance h' from the concave-down reflector, and the antenna beam illuminates a relatively large area (here called L). The power of the echo signal is significantly determined by the shape of the reflecting surface. In fact, if the reflector is approximately an arc (2-D model), with a radius of curvature ρ, and a point-image is at a distance r from the arc, the receiving antenna, of linear dimension (or rather, radius of capture area of the antenna) l, captures a power proportional to $1/l$ (Whitehead, 1956). Directly applying the optical geometry, Whitehead (1956) demonstrated that, if the antenna illuminates a large area, then the focusing reflector concentrates the power in a smaller area (at the point l) where the VIS system is positioned.

This focusing effect produces a gain G_f expressed by the formula:

$$G_f \approx 1/(1 - h'/\rho) \tag{6}$$

In the case of a convex-up arc reflector, there is a power loss of the same amount. If spherical reflectors are considered (3-D model), the gain is

$$G_f \approx 1/(1 - h'/\rho)^2 \tag{7}$$

Theoretically, to evaluate the contribution of focusing/defocusing reflectors on the received signal, an estimate must be made of the surface reflecting area and the geometrical parameters appearing in the Eq. (7). In contrast, by measuring the signal power variation, the quantity G_f can be determined. In the present case, by applying range gating, the reflecting area is in the order of one thousand square kilometers at maximum and the gain/loss is dependent on the curvature radius and the distance between the receiver and the reflector. In the described geometrical conditions, it was found that the coherent reflector shape can give 1–2 dB at maximum. From the power variation in the time sequences recorded it is possible to exclude the change from a convex to a concave reflector during the time period of the measurement. Only in case of MSTIDs or LSTIDs the temporal and spatial dimension of the irregularities can give contributions from 0 to a few dB (McNamara, 1991).

5. Frequency domain analysis of the echo signal

First, the amplitude excursion of the echo signal was evaluated from the different ionospheric layers, ranging from −94 dBm (noise floor in the instrument band of ≈60 kHz) to −67 dBm of the strongest echo signal. The range gating in the temporal data sequence ensures a nearly constant geometrical loss (a few tens of dB). Concerning absorption and polarization losses, variations less than 1 dB can be assumed because the frequency is low and the wave does not penetrate deeply into the ionospheric plasma. Hence, what remains is mainly the typical multipath fading behavior caused by traveling ionospheric irregularities and, to a not clearly quantifiable extent, the focusing–defocusing gain or loss of the shaped reflectors that is less important. With this in mind multipath and focusing–defocusing fading were considered among the causes of the power variations. The second cause is much less relevant in the present paper. In this paragraph, a connection between the multipath signal from moving reflectors and focusing–defocusing of the time dependent shape of the single reflector with SSD within the mentioned time period is considered. The continuous presence of the layer between the two VIS was also checked to ascertain that the fixed frequency wave employed was always reflected by the same layer. In the time interval of 1 hour four VIS and four PVH data files were collected for all the days during the measurement campaign. In dependence on the kind of reflection (one or more paths), the power variation in time exhibits a different statistics. From hour to hour in the same layer it is possible to observe power variation suggesting the same particular statistic (Nagakami–Rice or Rayleigh) as well as completely different statistics. Within the hour, the

same reflector can show different patterns and relative statistics. In general, there is no significant difference in received power trend at different hours or for different reflectors (Es, F1, or F2 layer). The received power ranges approximately from −64 to −97 dBm with an excursion of ≈33 dB over the various hours. As an example, Fig. 3 shows fading of the signal over time of four different 256 s time sequences recorded during one hour of VIS measurements.

In these close-to-controlled conditions of propagation the signal shows its statistical trend. Two kinds of statistical channels are easily detected: Rayleigh or Nagakami–Rice channels depending on the dominant reflectors. In the first case, many reflectors contribute almost equally to the echo power, while in the second case there is only one predominant path that contributes to the power strength values, in the presence of other small out-of-phase paths. To better examine these trends, the FFT analysis with 512 samples was involved. It was also useful applying a tapering function to eliminate the ringing due to the box effect. The analysis confirmed what stated above and a series of cases are reported in Figs 4–6. In the mentioned measurement campaign, only for a few Rayleigh statistics cases like those reported in Fig. 4, it was possible to determine a well established periodicity in the fading signal variations.

Fig. 5 shows the same analysis but for the Nagakami–Rice fading, relatively common in a small temporal segment of signal; as highlighted by the two cases shown in the figure, unlike the Rayleigh statistics, this kind of statistics often does not present any well-defined periodicity. In Fig. 6 are instead reported examples of the most common cases, with the two statistical trends appearing overlapped, where, besides periodicities of few seconds, main periodicities of tens of seconds are determined.

In order to obtain an overall characterization of the time fading variation, Fig. 7 shows the percentage of occurrence of the main periods given as output by the FFT analysis, obtained analyzing PVH sequences of echo signals for a generic (Rayleigh, Nagakami–Rice or mixed) ionospheric channel.

As expected, short time periodicities are much more frequent respect to longer periodicities. The results show that the power variations are dependent on the small time-space scale disturbances compatible with the SSD characteristics illustrated in Table 1, this being the most evident result of the analysis. The power variation forced by the SSDs originates the multipath fading in an unpredictable way, also for quiet geomagnetic/ionospheric conditions. Nevertheless, this does not exclude longer time periods compatible with MSTIDs and LSTIDs, which were however not considered in the present analysis.

6. Conclusion

With the aim to observe and study the fading variation due to propagation of small scale disturbances, a measurement campaign was performed at the ionospheric observatory of Rome using an experimental set-up derived from an ionosonde at fixed frequency and acquiring time sequences of the echo signal. The echo signal reflected by the ionospheric layer during the measurement campaign was analyzed, using the fading characteristics, to infer the kind and space-time evolution of ionospheric irregularities. In order to evaluate the contribution of the multipath signal alone in the observed power variations, VIS measurements were performed in controlled conditions. Analyzing the fading fluctuations due to the ionospheric time-variant channel permitted identification of a series of ionospheric characteristics. Three ionospheric layers (Es, F1, and F2) were selected, applying a range gating window to the acquired signal. This allowed to make some considerations on the echo signals received from a well defined iso-density ionospheric layer whose illuminated surfaces vary from tens to hundreds of square kilometers, this depending on the height of the analyzed ionospheric layer. Power variations of the order of a few dB up to tens of dB were found in a temporal segment of 256 s of echo signals. An initial analysis evaluated loss-gain from the shaped convex or concave coherent reflectors, where the surfaces involved, estimated by the range gating windows, had partially explained the observed power change in the echo signal. It was found that the shape of the coherent reflector gives ±1 or 2 dB, which is negligible with respect to the observed power variation easily reaching 35–40 dB. Simple geometrical evaluations together with the temporal power variation exclude the involvement of very large coherent reflecting surfaces. This confirms that the multipath signal of numerous reflectors contributes constructively or destructively in phase. Probably, the combination of the two mentioned phenomena better explains the power variations observed in the power versus time sequences even if multipath fading is much more relevant. It was found that short term fading is often associated to SSDs that do not present a well-defined periodicity. Each examined time sequence exhibited its own periodicity and fading characteristics, confirming that at this time-spatial scale the motions are largely chaotic and regular periodicity lasting the whole 256 s period considered in the analysis was seldom observed. It has been found that the observed fading can follow either the Rayleigh statistics, for which only one predominant path contributes to the power strength values, or the Nagakami–Rice statistics, for which many reflectors contribute almost equally to the echo power. Nevertheless, much more frequently the two statistics are simultaneously present. This experimental work confirmed that, in the time periods considered, fading follows a statistics mainly associated with SSDs, which is not predictable. At the time-space scale of SSDs we found that the irregularities do not maintain a coherent motion for periods of the order of tens of seconds.

References

Bianchi, C., Altadill, D. Ionospheric doppler measurements by means of HF-radars techniques. Ann. Geophys. 48 (6), 989–993, 2005.

Bianchi, C., Baskaradas, J.A., Pietrella, M., Sciacca, U., Zuccheretti, E. Power variation analysis of echo signals from ionospheric reflectors. Adv. Space Res. 51, 722–729, 2013.

Bianchi, C., Sciacca, U., Tabacco, E., Zirizzotti, A., Zuccheretti, E. On the shape of reflecting surfaces investigated by a 60 MHz radar. Int. J. Remote Sens. 24 (15), 3049–3058, 2003.

Blanc, E. Observations in the upper atmosphere of infrasonic waves from natural or artificial sources: a summary. Ann. Geophys. 3, 673–688, 1985.

Blaunstein, N., Plohotniuc, E. Ionosphere and Applied Aspects of Radio Communication and Radar, CRC Press, pp. 600, ISBN 9781420055146, 2006.

Crowley, G., Rodrigues, F.S. Characteristics of traveling ionospheric disturbances observed by the TIDDBIT sounder. Radio Sci. 47, RS0L22, http://dx.doi.org/10.1029/2011RS004959, 2012.

Francis, S.H. Global propagation of atmospheric gravity waves: a review. J. Atmos. Terr. Phys. 37, 1011–1054, 1975.

Hines, C.O. Internal atmospheric gravity waves at ionospheric heights. Canad. J. Phys. 38, 1441–1481, 1960.

James, H.G., Gillies, R.G., Hussey, G.C., Prikryl, P. HF fades caused by multiple wave fronts detected by a dipole antenna in the ionosphere, Radio Sci. 41, RS4018, http://dx.doi.org/10.1029/2005RS003385, 2006.

Kouris, S.S., Zolesi, B., Fotiadis, D., Bianchi, C. On the variability within-the-hour and from hour-to-hour of the F-region characteristics above Rome. Phys. Chem. Earth 25 (4), 347–351, 2000.

Krasnov, V., Yana, M., Drobzheva, V., Lastovicka, J. Recent advances and difficulties of infrasonic wave investigation in the ionosphere. Surveys Geophys. 27, 169–209, doi:10.1007/s10712-005-6203-4, 2006.

Leitinger, R., Rieger, M. The TID model for modulation of large scale electron density models. Ann. Geophys. 48 (3), 515–523, 2005.

McNamara, L.F. The Ionosphere: Communications, Surveillance, and Direction Finding. Krieger Pub. Co., pp. 237, 1991.

Pietrella, M., Zuccheretti, E. Coerenza: A software tool for computing the maximum coherence times of the ionosphere. Comput. Geosci. 36 (12), 1504–1511, http://dx.doi.org/10.1016/j.cageo.2010.03.020, 2010.

Proakis, G. Digital Communications. McGraw-Hill, 3rd ed., 1995.

Reinisch, B.W., Galkin, I.A. Global ionospheric radio observatory (GIRO). Earth Planets Space 63, 377–381, 2011.

Sklar, B. Digital Communications, Fundamentals and Applications, 2nd ed Prentice Hall, New Jersey, 2001.

Warrington, E.M., Bourdillon, A., Eulalia, B., Bianchi, C., Monilié, J.-P., Muriuki, M., Pietrella, M., Rannou, V., Rothkaehl, H., Saillant, S., Sari, O., Stocker, A.J., Tulunay, E., Tulunay, Y., Zaalov, N.Y. Aspects of HF radio propagation. Ann. Geophys. 52 (3/4), 301–321, 2009.

Whitehead, J.D. The focusing of short radio waves reflected from the ionosphere. J. Atmos. Terr. Phys. 9, 269–275, 1956.

Yau, K.S.B., Coleman, C.J., Cervera, M.A. Investigation on fading of high frequency radio signals propagating in the ionosphere – results from a Jindalee radar experiment. in: 10th IET International Conference on Ionospheric Radio Systems and Techniques, IET Conference, Publication Issue CP517 P.7-11, 2006.

Zuccheretti, E., Tutone, G., Sciacca, U., Bianchi, C., Baskaradas, J.A. The new AIS-INGV digital ionosonde. Ann. Geophys. 46 (4), 647–659, 2003.